Artificial photosynthetic reaction centers coupled to light-harvesting antennas

Pulak Kumar Ghosh,[1,*] Anatoly Yu. Smirnov,[1,2] and Franco Nori[1,2]
[1]*Advanced Science Institute, RIKEN, Wako-shi, Saitama 351-0198, Japan*
[2]*Department of Physics, The University of Michigan, Ann Arbor, Michigan 48109-1040, USA*
(Received 21 September 2011; published 22 December 2011)

We analyze a theoretical model for energy and electron transfer in an artificial photosynthetic system. The photosystem consists of a molecular triad (i.e., with a donor, a photosensitive unit, and an acceptor) coupled to four accessory light-harvesting-antenna pigments. The resonant energy transfer from the antennas to the artificial reaction center (the molecular triad) is described here by the Förster mechanism. We consider two different kinds of arrangements of the accessory light-harvesting pigments around the reaction center. The first arrangement allows direct excitation transfer to the reaction center from all the surrounding pigments. The second configuration transmits energy via a cascade mechanism along a chain of light-harvesting chromophores, where only one chromophore is connected to the reaction center. We show that the artificial photosynthetic system using the cascade energy transfer absorbs photons in a broader wavelength range and converts their energy into electricity with a higher efficiency than the system based on direct couplings between all the antenna chromophores and the reaction center.

DOI: 10.1103/PhysRevE.84.061138 PACS number(s): 05.60.Gg

I. INTRODUCTION

The reaction centers of natural photosystems are surrounded by a number of accessory light-harvesting complexes [1,2]. These light-harvesting antennas absorb sunlight photons and deliver their excitation energy to the reaction center, which creates a charge-separated state. The photosystem of green plants is made up of six photosynthetic accessory pigments: carotene, xanthophyll, phaeophytin *a*, phaeophytin *b*, chlorophyll *a*, and chlorophyll *b* [1]. Each pigment absorbs light in a different range of the solar spectrum. As a result, the antenna complex significantly increases the effective frequency range for the light absorption, resulting in a highly efficient photocurrent generation.

The efficient performance of natural photosystems motivates researchers to mimic their functions by creating photosynthetic units that combine antenna complexes with artificial reaction centers. For example, a light-harvesting array of metalated porphyrins was developed in Ref. [3]. This array absorbs light and rapidly transfers the excitation energy to the reaction center so that the porphyrin-fullerene (P-C_{60}) charge-separated state P^+-$C_{60}{}^-$ is formed with a quantum yield ∼70%. Mixed self-assembled monolayers of the ferrocene-porphyrin-fullerene molecular triad and the boron-dipyrrin dye (*B*) have been made in Refs. [4,5] with the goal to examine both energy and electron transfers in the artificial reaction center (Fc-P-C_{60}), coupled to the light-harvesting molecule *B*. A quantum yield of ∼ 50% for photocurrent production at a wavelength of 510 nm and a quantum yield of ∼21% at a wavelength of 430 nm have been reported [4].

A more efficient, sophisticated, and rigid antenna-reaction system was designed in Refs. [6,7]. This system includes three kinds of light-absorbing chromophores: (i) bis(phenylethynyl)anthracene (BPEA), which absorbs at a wavelength of 450 nm (blue region); (ii) boron-dipyrromethene (BDPY), having a strong absorption at 513 nm (green region); and (iii) zinc tetraarylporphyrin, which absorbs at both 418 and 598 nm. This study reports ∼100% quantum yield for the excitation transfer and ∼95% quantum yield for the generation of the charge-separated state P^+-$C_{60}{}^-$.

Theoretical studies of light-induced electron- and proton-pumping mechanisms [8,9] can be useful for a better understanding of (and for optimizing) light-to-electricity conversion, as well as for developing efficient designs of solar cells. Recently, we analyzed theoretically [10] the light-to-electricity energy conversion in a molecular triad (Fc-P-C_{60}) electronically coupled to conducting leads. It was shown that the Fc-P-C_{60} triad can transform light energy into electricity with a power-conversion efficiency of order of 40%, provided the connection of the triad to the leads is strong enough. It should be noted, however, that this prototypical solar cell absorbs photons with energies in close proximity to the resonant transition of the central porphyrin molecule. Therefore, a major fraction of the sunlight spectrum is not converted to the electrical form by this device.

In this paper we examine a theoretical model for the light-to-electricity energy conversion by a molecular triad, which is surrounded by four additional light-harvesting antenna complexes. We show that this artificial photosystem is able to generate a photocurrent with a quantum yield of the order of 90% (when the reorganization energy for the resonant energy transfer is relatively high) absorbing photons in a wide range (420–670 nm) of the solar spectrum. We consider two different configurations for the antenna complexes: (a) one in which each light-harvesting molecule is independently connected (by the Förster energy-transfer mechanism) to the central porphyrin molecule of the triad [Fig. 1(a)] and (b) one in which the light-harvesting molecules are arranged in a line [Fig. 1(b)], with only one molecule directly coupled to the porphyrin and with other molecules forming a chain where the energy propagates in a cascadelike manner.

Resonant energy transfer in multichromophoric light-harvesting complexes has been studied theoretically in Refs. [2,11–14]. There, a reaction center is modeled phenomenologically as a set of exciton traps. Here we provide

*Author to whom correspondence should be addressed: pulak@riken.jp

a more detailed model of a reaction center, which directly converts light energy to an electric current.

Let us consider a [donor-porphyrin-acceptor (D-P-A)] reaction center surrounded by several (say, four) accessory light-harvesting antennas. A complex comprised of four antenna chromophores attached to the porphyrin-fullerene reaction center (RC) was synthesized and investigated in Ref. [15]. Recently, a complex comprised of five porphyrin antennas attached to the control unit was synthesized in Ref. [16]. Note that our theoretical approach can be applied to any number of antenna chromophores coupled to the reaction center. Even with four antennas, many possible configurations of our photosystem could be considered. However, to simplify this analysis, we will now focus on two extreme cases, with somewhat opposite topologies or networks: a well-connected reaction center (directly connected to *all* four accessory light-harvesting antennas) and the opposite case in which the central reaction center is coupled to *only one* antenna, which is now part of a linear chain. These two extreme-opposite topologies or networks can be denoted as star shaped [shown in Fig. 1(a)] and a linear chain [Fig. 1(b)], respectively. The star-shaped topology can be implemented in the manner shown in Ref. [16], whereas for synthesizing the linear-chain antenna complex experimentalists could use the procedure described in Ref. [15]. In the latter case this is sufficient to create only one-half of the antenna from Ref. [15] containing a chain BPEA → BDPY → ZnPy → RC (see also Refs. [17,18]).

Our goal is to find the best way to place these accessory antennas, when more energy is transferred from the antennas to the reaction center and more energy is converted to electricity. The two issues considered here are (i) how to physically arrange antennas around the central reaction center and (ii) how to arrange these in *energy space*. The first issue is topological and focuses on the network connectivity in real space: for instance, how many accessory antennas are connected to a central reaction center. The second issue refers to the *energy match* (or mismatch) between neighboring antennas and between them and the central reaction center. A large energy mismatch between any connected units in the chain would preclude energy transfer between them. This approximate energy-matching issue between neighboring units is equally important to keep in mind, not just the real-space topological arrangement of the units. We consider antenna complexes consisting of light-absorbing molecules (BPEA, BDPY, and porphyrins) with definite resonant energies. These chromophores are extensively used in experiments [6,7,15].

Figure 1 shows the connectivity between the different units: (a) star-shaped topology and (b) linear-chain configuration. Moreover, the colors there represent, very schematically, the energy range where each unit operates optimally. The linear chain shown there has antennas arranged in a way that nearby units operate in approximately similar energy ranges. This energy-matching issue perhaps is not very clear in Fig. 1, even when seen in color. The energy scales are shown far more explicitly in Fig. 2. Figure 2(b) clearly shows that the linear-chain model considered here operates via an energy cascade, or linear-chain reaction, like a line of falling dominoes, one event triggering the next one, in a sequential manner, with small energy mismatches between successive energy-transfer events. As shown in Fig. 2(b), the more energetic antenna

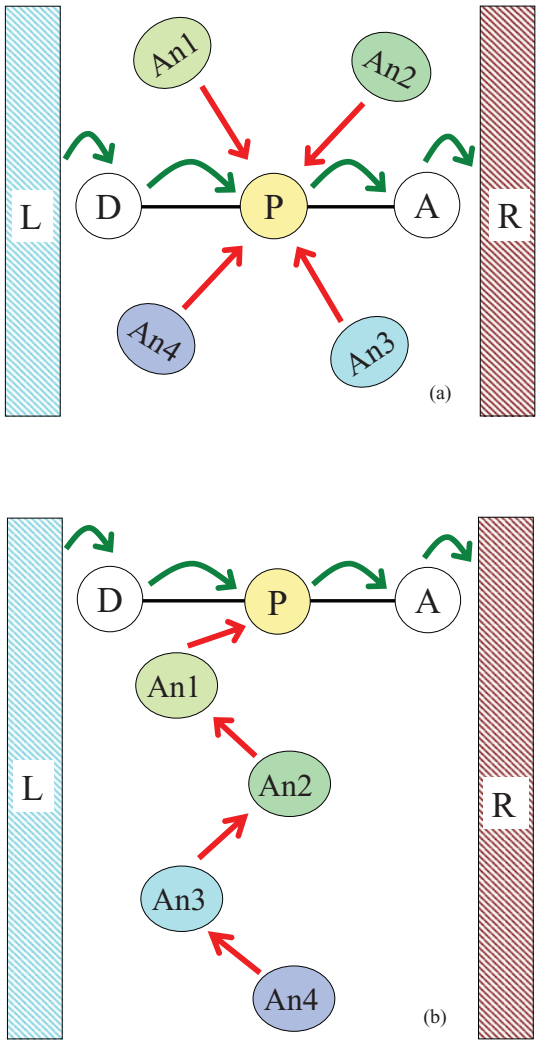

FIG. 1. (Color online) Schematic diagram of an artificial photosystem comprised of a molecular triad (D-P-A) and four additional light-harvesting complexes (An1, An2, An3, An4). Here D denotes the donor, A denotes the acceptor, and P denotes the photosensitive part (porphyrin). The molecular triad D-P-A is inserted between two electrodes (leads) L and R. Energy exchange processes are denoted by straight (red) arrows. The curved (green) arrows describe electron pathways L → D → P → A→ R via the molecular triad. (a) The photosensitive part P of the molecular triad is surrounded by four accessory light-harvesting complexes An1, An2, An3, and An4. In this case the surrounding antenna complexes can transfer excitations to the reaction center directly. (b) The antenna complexes form a linear chain coupled to the reaction center via nearest-neighbor couplings.

is located far away from the reaction center and is coupled to an antenna with a slightly lower energy, which is coupled to another antenna with an even slightly lower energy, and so on, moving energetically downhill along the chain. Thus the neighboring antennas must be so in both real space and *also* energy space to allow for the efficient transfer of energy between them. Thus proximity between units must be in two spaces: real space and energy space.

This paper is organized as follows. In Sec. II we outline a model for the artificial reaction center (molecular triad) coupled to the antenna complex. We briefly describe our

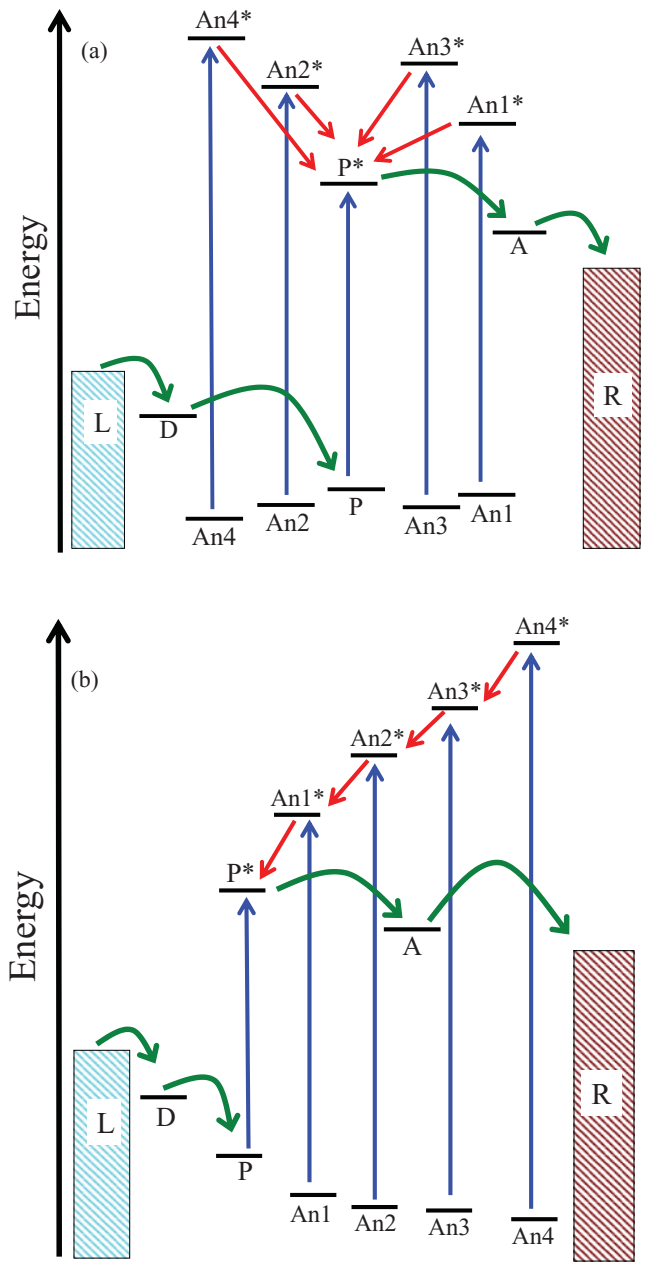

FIG. 2. (Color online) Energy diagram of the antenna complexes An1, . . . ,An4, energetically coupled to the reaction center D-P-A for the case in which (a) each light-harvesting molecule is directly connected to the porphyrin molecule P of the RC and (b) the energy transfer occurs via a linear chain of antennas with nearest-neighbor energy exchange. Note that the four antenna chromophores in (b) are arranged in such a way that there is a relatively small energy difference between neighboring units.

mathematical methods in Sec. III. The parameters are listed in Sec. IV. In Sec. V we solve numerically the master equations and analyze the energy-transfer process. A summary is presented in Sec. VI. The methods used are described in more detail in Appendixes A and B.

II. MODEL

We start with a schematic description of the energy- and electron-transfer processes in an artificial reaction center D-P-A combined with four antenna chromophores: An1, An2, An3, and An4 [see Figs. 1(a) and 1(b), which show two different configurations for these antennas: a star-shaped configuration in Fig. 1(a) and a chain in Fig. 1(b)]. The photosensitive molecular triad D-P-A is inserted between two electron reservoirs (electrodes) L and R. The donor D is coupled to the left lead L and the acceptor A is connected to the right lead R. As in Refs. [4,10], the donor and acceptor molecules (e.g., ferrocene and fullerene) are connected to each other via the photosensitive molecule (porphyrin P). This molecule is surrounded by four accessory light-harvesting pigments (ALHPs). Figure 1(a) corresponds to the situation where all pigments are directly coupled to the photosensitive part P of the molecular triad. In this star-shaped geometric arrangement, all the ALHPs can directly transfer excitations to the photosensitive part of the molecular triad. Figure 1(b) corresponds to the case in which the light-harvesting pigments form a chain, which transfers energy where the excitation moves from one pigment to the next one via nearest-neighbor couplings: An4 $\rightarrow$ An3 $\rightarrow$ An2 $\rightarrow$ An1 $\rightarrow$ P. This cascadelike excitation transfer occurs in an energetically downhill direction, akin to a one-dimensional chain reaction or domino effect.

Figures 2(a) and 2(b) present energy diagrams of the photosystems described in Figs. 1(a) and 1(b), respectively. The electron transfer chain L $\rightarrow$ D $\rightarrow$ P $\rightarrow$ P* $\rightarrow$ A $\rightarrow$ R is the same for both configurations (a) and (b) and both begin on the left lead L. The electrochemical potentials of the left and right electron reservoirs are determined by the parameters μ_L and μ_R, with $\mu_R > \mu_L$. Since the energy level E_D of the donor D is lower than the potential μ_L of the left lead, $E_D < \mu_L$, electrons can move from the L reservoir to level D and afterward to the low-lying ground-state energy level E_P of the porphyrin. When absorbing a photon, the electron in the porphyrin molecule jumps from its ground state P to its excited state P*. A subsequent electron transfer from P* to the acceptor A is driven by a negative-energy gradient $E_A - E_{P^*} < 0$. In view of the relation $E_A > \mu_R$, the electron in A is finally transferred to the right R electron reservoir. This is the light-induced electron transition in the porphyrin molecule, which results in an energetically uphill electron flow in both photosynthetic systems (a) and (b).

Even though these systems (a) and (b) have similar electron-transport chains, their light-harvesting complexes are arranged quite differently. Each of these complexes An = An1, . . . ,An4 can be characterized by ground-state E_{An} and an excited-state E_{An^*} energy levels with an energy difference $\omega_{\mathrm{An}} = E_{\mathrm{An}^*} - E_{\mathrm{An}}$. Hereafter we assume that $\hbar = 1$ and $k_B = 1$. For light-harvesting complex (a) [see Figs. 1(a) and 2(a)], all frequencies $\omega_{\mathrm{An1}}, \ldots, \omega_{\mathrm{An4}}$ should exceed the porphyrin transition frequency $\omega_P = E_{P^*} - E_P$. In this case the energy of photons collected by each individual antenna can be transferred directly to the photosensitive part of the artificial reaction center (porphyrin molecule). However, in light-harvesting complex (b) [see Figs. 1(b) and 2(b)], only the antenna An1 is coupled (by a Förster mechanism) to the porphyrin, whereas the other light-harvesting pigments form a linear chain that transfers energy downhill along the chain: An4 $\rightarrow$ An3 $\rightarrow$ An2 $\rightarrow$ An1 $\rightarrow$ P. This energy transfer can be energetically allowed provided $\omega_{\mathrm{An4}} > \omega_{\mathrm{An3}} >$

$\omega_{An2} > \omega_{An1} > \omega_P$. In Sec. V we compare these two artificial photosystems and determine which arrangement of the antenna complexes provides more energy to the reaction center.

III. METHODS

The electron flow through a molecular triad coupled to two electron reservoirs can be described with methods of quantum transport theory and the theory of open quantum systems (see, e.g., Refs. [10,19,20]). In addition to four sites (D, P, P*, and A) describing the molecular triad, we introduce four pairs (An1, An1*, ..., An4, An4*) that characterize the ground and excited states of the light-harvesting antennas.

The total Hamiltonian H of the system should include the two most important parts: (i) H_0, the Hamiltonian of the electron sites and leads, including the Coulomb interaction between the electrons located on different sites of the triad and (ii) H_{Forster}, which, in the case of the design in Fig. 1(a), includes the direct resonant coupling between the porphyrin molecule P and the light-harvesting complexes An1, ..., An4. In addition, we have to take into consideration the Hamiltonians H_{tr} and H_{tun}, which describe tunneling between the electron sites on the triad and the electron reservoirs and tunneling between the electron-binding sites belonging to the molecular triad, respectively. The interaction H_{light} of the porphyrin molecule and antenna complexes with an external electromagnetic field (laser field) should also be considered because of the energy dissipation due to the interaction of the antenna complex with the environment and especially with the blackbody radiation heat bath.

As in the experimental situation [6], we assume that a radiationless energy-transfer mechanism, described by the Förster dipole-dipole matrix element (see Refs. [2,11,21] and references therein)

$$V_{kl} = -\frac{1}{4\pi\epsilon_0\epsilon R_{kl}^3}\left[\mathbf{d}_k\cdot\mathbf{d}_l - 3\frac{(\mathbf{d}_k\cdot\mathbf{R}_{kl})(\mathbf{d}_l\cdot\mathbf{R}_{kl})}{\mathbf{R}_{kl}^2}\right], \quad (1)$$

is mainly responsible for exciton propagation between chromophores k and l, separated by the nanoscale distance $R_{kl} = |\mathbf{R}_{kl}|$. Here ϵ_0 is the vacuum dielectric constant and ϵ is the dielectric constant of surroundings. The matrix element V_{kl} depends on the orientations of the dipole moments $\mathbf{d}_k$ and $\mathbf{d}_l$ of the pigments with respect to the vector $\mathbf{R}_{kl}$ between chromophores. The same mechanism provides the energy transfer between the nearest neighbors in the antenna chain, as well as between the complex An1 and the porphyrin molecule in the linear-chain configuration shown in Fig. 1(b). To estimate the value of the Förster coupling we can use a simpler formula [22] $V_F = V_{kl} \sim d_k d_l/2\pi\epsilon_0\epsilon R^3$. This simplified formula is obtained by assuming a parallel orientation of the respective dipole moments and coordinate vectors.

It should be emphasized that here we are interested in the steady-state regime of light-to-electricity energy conversion in the molecular triad coupled to the antenna complex. To describe this regime we use solutions of the master equations (see Appendixes A and B) taken in the long-time limit. Quantum coherence effects do not play any significant role in the process since the decoherence time is expected to be in the subpicosecond range even at low temperatures (see, e.g., Refs. [23–25]), whereas the time scale for the energy and charge transfer exceeds a few picoseconds [6,15]. Our master equations are derived when the coupling amplitudes between chromophores V_F and tunneling amplitudes Δ are smaller than the reorganization energies (which describe an interaction of the system with the environment [10,19,20]). A standard Redfield approach [26] is able to describe quantum oscillations; however, it does not work for strong system-bath couplings.

IV. PARAMETERS

A. Energy levels and electrochemical potentials

The energy levels of the Fc-P-C_{60} molecular triad are $E_D = -510$ meV, $E_P = -1150$ meV, $E_{P^*} = 750$ meV, and $E_A = 620$ meV. These values are obtained by estimating the reduction potentials (using a reference electrode Ag-AgCl) of ferrocene D, porphyrin P and P*, and fullerene A molecules [27]. For the electrochemical potentials of the left μ_L and the right μ_R leads, we choose the following values: $\mu_L = -410$ meV and $\mu_R = 520$ meV, with the electrochemical gradient $\Delta\mu = \mu_R - \mu_L = 930$ meV.

B. Coulomb interactions

The spatial separations between D-P, P-A, and D-A are of order of 1.62, 1.8, and 3.42 nm, respectively [27]. The Coulomb energies u_{DP}, u_{DA}, and u_{PA} can be calculated with the formula

$$u_{ij} = \frac{e^2}{4\pi\epsilon_0\epsilon r_{ij}},$$

where $\{ij\} = \{\text{DP}\},\{\text{DA}\},\{\text{PA}\}$; e is the electron charge; and ϵ_0 is the vacuum dielectric constant. For $\epsilon \sim 4.4$, the Coulomb interaction energies are $u_{DP} = 200$ meV, $u_{DA} = 95$ meV, and $u_{PA} = 180$ meV.

The Förster coupling $V_F = V_{kl}$ between the photosensitive molecules k and l is estimated as $V_F \sim 7$ meV, if the dipole moments of the pigments satisfy $d_k \sim d_l \sim 0.1\ e$ nm, and the distance $R_{kl} \sim 1$ nm.

C. Tunneling amplitudes

We have assumed that the ferrocene-porphyrin and porphyrin-fullerene tunneling amplitudes are about ~3 meV, so that

$$\frac{\Delta_{DP}}{\hbar} = \frac{\Delta_{DP^*}}{\hbar} = \frac{\Delta_{AP}}{\hbar} = \frac{\Delta_{AP^*}}{\hbar} = 4.5\text{ps}^{-1}.$$

For the tunneling rate Γ_L between the left lead (gold) and ferrocene, we choose the value $\Gamma_L/\hbar = 1800\ \mu\text{s}^{-1}$, which follows from the experimental measurements [28] of the energy-independent ferrocene-gold tunneling factor $|T_{kL}| \sim |T_{kL}| = 6.5\ \text{cm}^{-1}$ and from the formula in Eq. (B4) in Appendix B calculated at the electron density $\rho(\epsilon_F) \sim 0.3\ \text{eV}^{-1}\,\text{atom}^{-1}$ for the states of gold at the Fermi energy $\epsilon_F = 5.51$ eV. For the parameter Γ_R, we use the optimal value $\Gamma_R/\hbar = 180\ \mu\text{s}^{-1}$, obtained in Ref. [10].

D. Radiation leakage and quenching rates

We take the following estimates for the radiation leakage time: $\tau_{P^*\to P} = \tau_{P^*\to D} = \tau_{A\to P} \sim 0.4$ ns. Similar estimates

have been used for the radiation leakage time scales of the antenna molecules. For the quenching (or energy-loss) time of the porphyrin excited state P* we use the value $\tau_{\rm quen} \sim 0.1$ ns.

E. Reorganization energies for the electron and energy transfers

For the molecular triad analyzed in Ref. [10] we obtain the relatively high power-conversion efficiency $\eta \sim 42\%$ provided the donor-porphyrin and acceptor-porphyrin electron-transfer reorganization energies are about $\Lambda_{DP} \sim 600$ meV and $\Lambda_{AP} \sim 100$–400 meV. These values are close to the parameters reported in Refs. [29,30]. A much smaller value $\Lambda_{PP*} \sim 100$ meV is assumed for the light-induced electron transitions between the ground P and excited P* levels of the porphyrin molecule. The Förster energy transfer between the light-harvesting molecules and between these molecules and the porphyrin is also accompanied by an environment-reorganization process, which can be characterized by a smaller energy scale $\Lambda_F \leqslant 100$ meV (see, e.g., the energy transfer in the B850 complex [31], where Λ_F is assumed to be about 30 meV).

Hereafter, we assume that the external light source has a fixed intensity $I = 100$ mW/cm^2 and that the environment is kept at room temperature $T = 298$ K. We also assume that the reorganization energy for the Förster energy transfer Λ_F is about 100 meV unless otherwise specified. We analyze the Fc-P-C_{60} molecular triad, where the ferrocene molecule Fc is attached to the gold surface (left lead L), and the fullerene C_{60} is in contact with an electrolyte solution (right lead R) filled with oxygen molecules, which are able to accept electrons from the C_{60} molecules.

V. RESULTS AND DISCUSSION

We derive and solve numerically a set of master equations for the probabilities to find the system in a definite eigenstate of the basis Hamiltonian. This is explained in Appendix B. After that we calculate the energetically uphill electron current through the triad and the energy of the photons absorbed by the triad and by the light-harvesting molecules. This allows us to determine a quantum yield and power-conversion efficiency of the system (see all definitions in Appendix C).

A. Photocurrent through the molecular triad directly coupled to four porphyrin light-harvesting molecules

Here we consider the situation in which both the reaction center and the antenna complexes are made of porphyrin molecules with the geometrical arrangement shown in Fig. 1(a). This arrangement allows direct energy transfer from each light-harvesting chromophore to the reaction center.

In Fig. 3 we plot the photocurrent through the triad as a function of the wavelength of light for different values of the Förster coupling strength $V_F = 0$, 0.1, 1, and 10 (in meV) and for the above-mentioned set of parameters of the system. It is apparent from Fig. 3 that the magnitude of the light-induced pumping current at $\lambda = 620$ nm is significantly enhanced (about 5 times larger when $V_F = 10$ meV) by the antenna system. However, the spectral range of the light absorption remains the same as for the detached porphyrin reaction center [see Fig. 3, where the (black) curve with square symbols describes the photocurrent through the molecular triad completely disconnected from the antenna chromophores $V_F = 0$]. We also find that the quantum yield Φ taken in the middle of the resonant peak ($\lambda = 620$ nm) *nonmonotonically* depends on the Förster coupling strength V_F measured here in meV: $\Phi(V_F = 0) \simeq 0.85, \Phi(0.1) \simeq 0.3, \Phi(1) \simeq 0.75$, and $\Phi(10) \simeq 0.82$. It is evident from Eq. (B6) that the excitation-energy-transfer rate is proportional to the square V_F^2 of the Förster coupling. Therefore, the efficiency of the excitation-energy-transfer processes between the antenna complexes and the reaction center should also be proportional to V_F^2. For a sufficiently large Förster coupling, the bottleneck of the overall energy-transfer process lies in the charge-transfer processes. Thus the excited states of the antenna chromophores need to wait in order to create a charge-separated state of the reaction center due to the limited capacity of the electron-transfer chain. As a result, the energy transduction efficiency does not increase linearly with the square of V_F.

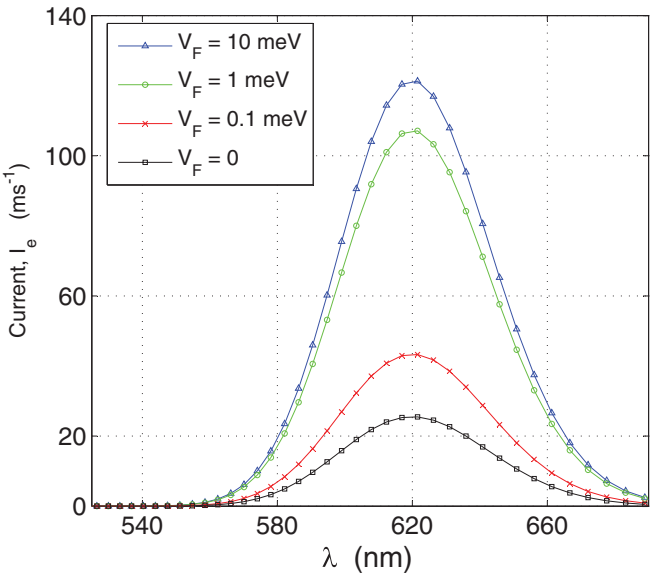

FIG. 3. (Color online) Photoinduced electron current I_e (number of electrons pumped from the L to the R lead in 1 ms) versus the wavelength of the incident light for a photosystem with four antenna complexes, which are made of porphyrin molecules. Both the antenna complexes and the reaction center absorb at the same wavelength. The whole complex now absorbs more photons than the single porphyrin molecule, thus pumping many more electrons from the left (with $\mu_L = -410$ meV) to the right (with $\mu_R = 520$ meV) electron reservoir. The other parameters are listed in the text (see Sec. IV). The peak in the current increases for larger values of the Förster coupling strength V_F. We also studied (not shown here) higher values of V_F, but these produced the same results as $V_F = 10$ meV. Thus this value of V_F provides a saturation in the electron current. The resonant peak here is $\lambda = 620$ nm. It follows from Eq. (B8) that the light-induced excitation rate of porphyrin P is maximized when $\omega_0 = \Delta E_{PP*} + \Lambda_{PP*} \sim 2000$ meV, which corresponds to the resonance peak around 620 nm.

B. Molecular triad connected to two BPEA and two BDPY chromophores

Now we consider a different case: an antenna system comprised of two BDPY and two BPEA molecules. The BDPY molecule has the maximum absorbance in the green region (at 513 nm) of the solar spectrum, where neither BPEA (with maximum absorbance at 450 nm) nor the porphyrin, which absorbs at 620 nm, have maxima of absorption spectra. It should be noted that a multichromophoric hexad antenna system having three light-absorbing BDPY, BPEA, and porphyrin molecules has been developed in Ref. [6], where the charge-separated state P^+-$C_{60}{}^-$ has been generated with almost 95% quantum yield [6]. In our case, the porphyrin unit of the molecular triad is coupled to the four antenna chromophores (two BDPY and two BPEA).

We consider two situations: (a) one in which the antenna chromophores are *directly* coupled to the porphyrin unit of the reaction center [Figs. 1(a) and 1(b)] one in which the antenna chromophores are *arranged in line*: BDPY → BDPY → BPEA → BPEA → RC, with the nearest-neighbor coupling between chromophores [see Fig. 1(b)]. Thus configuration (a) might appear to be energetically more efficient than (b). However, our calculations below indicate that this is not the case.

For the case (a) of direct connection between the four antenna chromophores and the triad [see Figs. 1(a) and 4] we calculate a photocurrent and a quantum yield Φ as functions of the wavelength of light at $\Lambda_F = 100$ meV and at four values of the Förster coupling $V_F = 0$,1,25, and 50 meV. The wavelength dependence of the current has two maxima centered at 513 and 620 nm. The BPEA molecules, which absorb at 450 nm, give a negligible contribution to the current since their spectral maxima are too far from the absorbance maximum of the porphyrin spectrum. As a consequence, the BPEA-porphyrin energy transfer is significantly suppressed at moderate values of the Förster reorganization energy $\Lambda_F \leqslant 100$ meV in the range of the coupling constants $V_F \leqslant 50$ meV. It follows from Fig. 4 (see the peak at $\lambda = 513$ nm) that the BDPY molecules start working as efficient light harvesters only at sufficiently strong Förster coupling $V_F \geqslant 10$ meV to the porphyrin unit of the molecular triad. We also note that when $\lambda \sim 513$ nm, both the photoinduced current and the quantum yield grow with increasing Förster coupling strength so that the quantum yield Φ can be around 48%. In the range of porphyrin absorption (at $\lambda \sim 620$ nm and $V_F = 0$) the quantum yield is of the order of 90%.

For case (b) a much broader light spectrum can be converted into electrical current in the linear configuration in Fig. 1(b), where the light-harvesting chromophores are arranged along a line BPEA → BPEA → BDPY → BDPY → RC, with the only one BDPY molecule directly coupled to the porphyrin unit of our artificial reaction center [see Figs. 1(b) and 5]. This system is able to collect photons in the range of wavelength from 420 nm up to 650 nm covering a significant part of the visible sunlight spectrum. The chain of BPEA and BDPY molecules creates an efficient channel, which gradually transmits energy from the collectors of high-energy photons (BPEA molecules), via the intermediate BDPY antennas, to the molecular triad. In Figs. 5(a) and 5(b) we plot the photoinduced current and the quantum yield versus the wavelength of the external radiation at $\Lambda_F = 100$ meV and at four values of the Förster constants (in meV) $V_F = 0$, 1,25,and 50. For large value of the Förster coupling strength V_F the quantum yield Φ reaches ∼48% in Fig. 4(a) around $\lambda = 513$ nm [for the star-shaped topology in Fig. 1(a)] and ∼30% in Fig. 5(b) [for the linear-chain case in Fig. 1(b)]. The quantum yield in Fig. 5(b) is lower than the one in Fig. 4(a), but extends over a wider range of wavelengths including the peaks at $\lambda \sim 450$ and 513 nm.

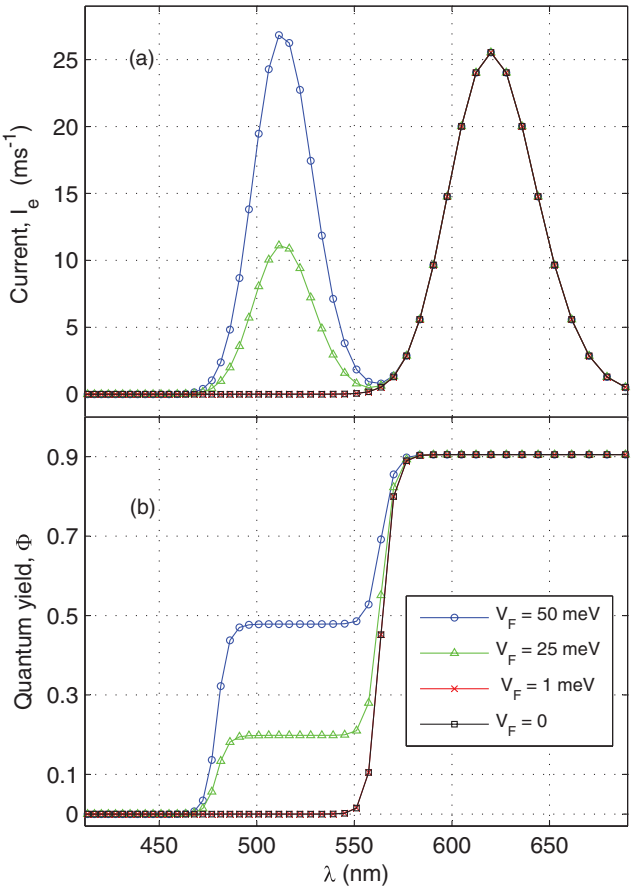

FIG. 4. (Color online) (a) Electron current I_e and (b) quantum yield Φ as functions of the wavelength λ of the external radiation for the configuration shown in Fig. 1(a), where two BPEA and two BDPY antenna chromophores are directly coupled to the centrally located reaction center. The Förster coupling constant V_F, which is assumed to be the same for every chromophore-RC connection, takes four values (in meV) $V_F = 0$, 1, 25, and 50. For other parameters see Sec. IV. Note that the electron current and the quantum yield grow for increasing values of the Förster coupling energy strength V_F. More importantly, the direct coupling [Fig. 1(a)] suppresses the peak at $\lambda = 450$ nm (a), which is present in the linear chain configuration [Fig. 1(b)], as shown in Fig. 5(a).

It follows from Figs. 4 and 5 that the configuration using the chainlike nearest-neighbor coupling between light-harvesting chromophores [Fig. 1(b)] converts much more blue ($\lambda = 450$ nm) light into electricity with a higher quantum yield than the star-shaped configuration with direct coupling between the antenna chromophores and the RC [Fig. 1(a)]. In this star-shaped configuration, the BPEA molecules, which collects blue photons, are *not* able to transfer their energy to the

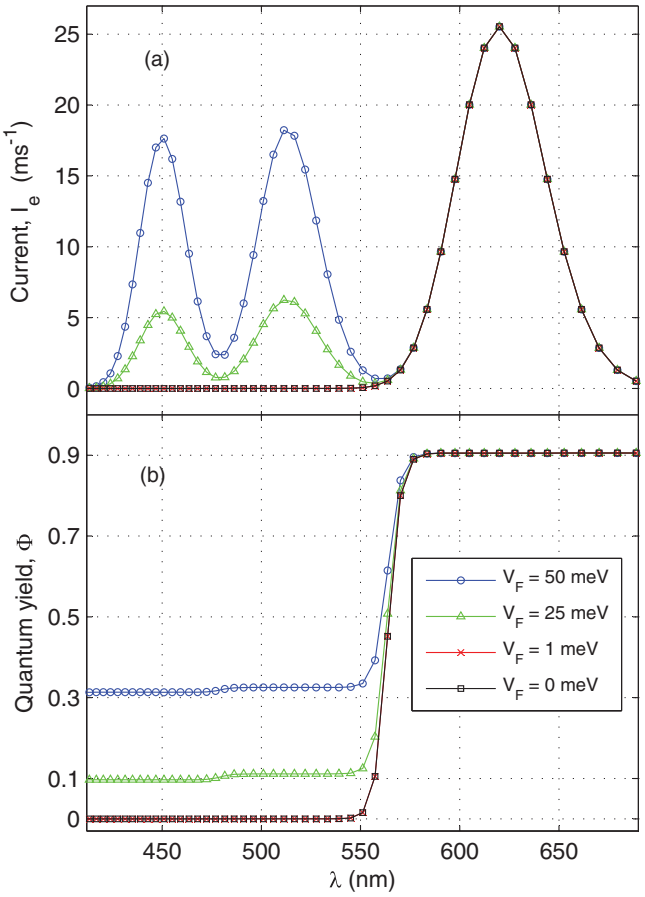

FIG. 5. (Color online) Electron current I_e and a quantum yield Φ versus the wavelength of light λ for the configuration shown in Fig. 1(b), where the excitation energy moves along the following chain of light-harvesting molecules: BPEA → BPEA → BDPY → BDPY → RC. The parameters used here are the same as in Fig. 4. However, the current peak at $\lambda \sim 450$ nm is present in (a) here, but absent in Fig. 4(a), which used a direct-coupling configuration to the central reaction center.

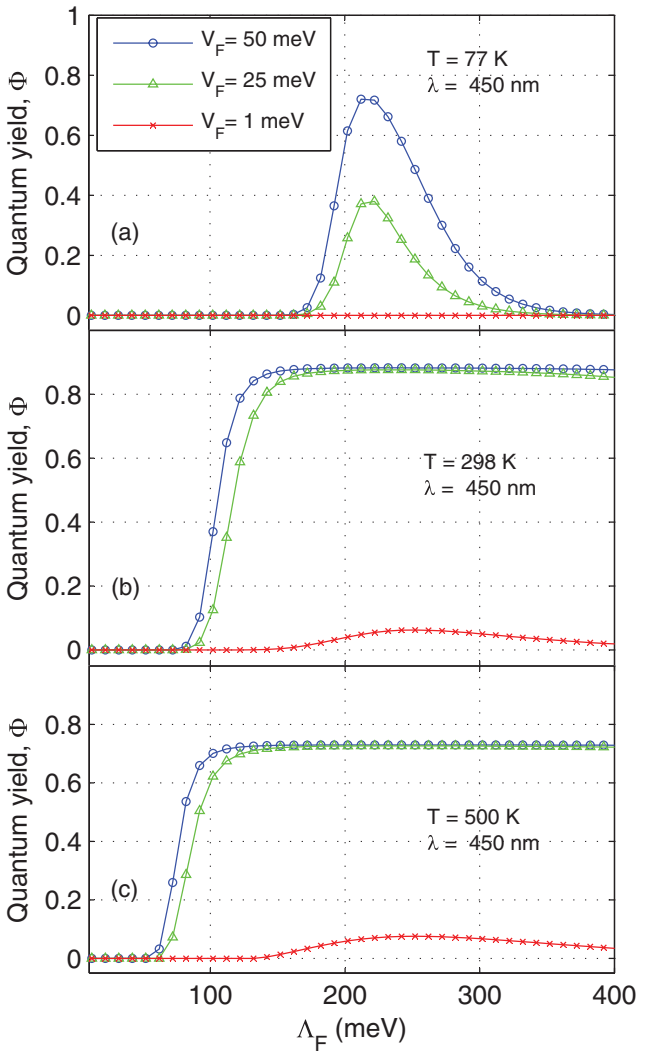

FIG. 6. (Color online) Quantum yield as a function of reorganization energy Λ_F for the linear-chain nearest-neighbor coupling between chromophores, BPEA → BPEA → BDPY → BDPY → RC, for the wavelength of light $\lambda = 450$ nm [blue peak in Fig. 5(a)] and three different temperatures: (a) low $T = 77$ K, (b) room temperature $T = 298$ K, and (c) very high $T = 500$ K, as well as for three values of the Förster constant $V_F = 1$,25, and 50 meV. As shown in (b) and (c), increasing the reorganization energy Λ_F can sharply increase the quantum yield. The extreme low-temperature case in (a) is just a limit case, shown for comparison with the higher-temperature cases in (b) and (c).

photosensitive unit of the triad due to a significant difference between the energies of the BPEA antennas ($\lambda = 450$ nm) and the porphyrin-based reaction center ($\lambda = 620$ nm).

The antenna-RC energy transfer is facilitated by the strong coupling to the environment (when the energy difference is high), which is characterized by the reorganization energy Λ_F, and by a tight Förster binding between chromophores, which is described by the constant V_F. In Figs. 6 and 7 we plot the quantum yield Φ as a function of the reorganization energy Λ_F for three different temperatures (in K): $T = 77$, 298, and 500 and for three values of the coupling constant $V_F = 1$,25, and 50 meV. Figure 6 is related to the blue peak of the absorption spectrum ($\lambda = 450$ nm), whereas figures 7 describes the behavior of the green peak ($\lambda = 513$ nm). The peak centered at $\lambda = 620$ nm is produced by the porphyrin molecule, belonging to the triad, and therefore shows no dependence on Λ_F and V_F.

The Marcus rates, which describe the energy transmission between the photosensitive elements of the system, depend on (i) the energy difference ΔE between the photosensitive units, (ii) the Förster coupling V_F, and (iii) the Förster reorganization energy Λ_F. The large energy separation ΔE of the energies of the nearby photosensitive molecules leads to a decrease of the Marcus rates and thus to the suppression of the energy transfer. In our case, the energy distance between the BPEA ($\lambda = 450$ nm) and BDPY ($\lambda = 513$ nm) molecules is about 340 meV, whereas the energy separation of the BDPY chromophore and porphyrin ($\lambda = 620$ nm) is of order of 415 meV. This energy gap can be partially compensated for by the large reorganization energy Λ_F, which reflects the significant fluctuations of the relative positions of the energy levels. Here the environment plays a positive role in assisting the efficient and fast energy

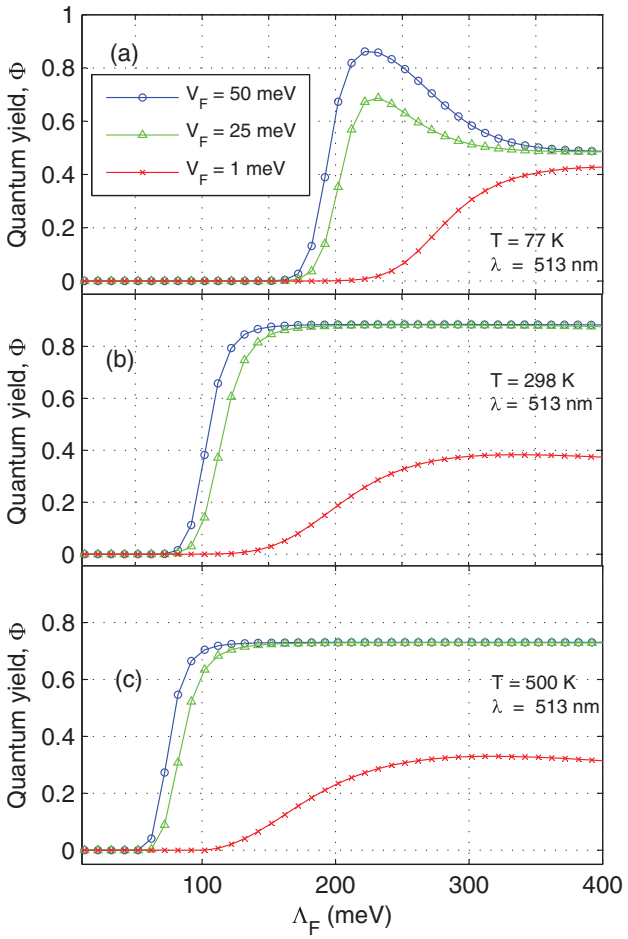

FIG. 7. (Color online) Quantum yield versus reorganization energy Λ_F for the peak of the spectrum at $\lambda = 513$ nm (green region) [see Fig. 5(a)] for three values of the Förster constant $V_F = 1, 25$, and 50 meV and at three different temperatures: (a) $T = 77$ K, (b) $T = 298$ K, and (c) $T = 500$ K. The other parameters are listed in Sec. IV. Figures 5–7 focus on the linear-chain configuration [Fig. 1(b)] with nearest-neighbor couplings between chromophores. Figures 6 and 7 show the same quantities, but centered at different peaks ($\lambda \sim 450$ nm versus $\lambda \sim 513$ nm).

transfer between chromophores (see also Refs. [11,13,26]). The time scales for the energy and electron transfers should be shorter than the radiation leakage time and the quenching time; otherwise, the energy of the photons absorbed by the system will be lost.

At low temperatures (e.g., liquid nitrogen, $T = 77$ K), the fluctuations in the positions of the energy levels of the chromophores are frozen, so the light-to-electricity conversion requires sufficiently large values of the reorganization energy $\Lambda_F > 180$ meV [see Figs. 6(a) and 7(a)]. Note that for $V_F > 25$ meV the linear-chain arrangement system has an optimal performance at $\Lambda_F \simeq 225$ meV for both frequency ranges. This extreme low-temperature case is only shown for comparison with the higher-temperature cases.

At room temperature ($T = 298$ K) and at strong enough Förster coupling $V_F \geqslant 25$ meV, the blue and green spectral peaks demonstrate similar behaviors as functions of Λ_F [see Figs. 6(b) and 7(b)]. Here the quantum yield begins to grow when the reorganization energy exceeds ~ 80meV, reaching finally 90% at $\Lambda_F > 150$ meV. These numbers are determined by the parameters of the antenna-triad complex and especially, by the radiation leakage time $\tau_{\rm rad}$ of the excited porphyrin state P*, estimated above as $\tau_{\rm rad} \sim 0.4$ ns.

At high temperatures (see Figs. 6(c) and 7(c), plotted for $T = 500$ K] the facilitating effect of the environment increases and the efficient energy transfer starts at the lower reorganization energies $\Lambda_F \geqslant 75$ meV. This value of Λ_F is comparable to the reorganization energy for the energy transfer in the B850 light-harvesting complex, where $\Lambda_F \simeq 27$ meV [31]. At the smaller value of the Förster coupling $V_F = 1$ meV the conversion of the blue light ($\lambda = 450$ nm) to electricity is significantly suppressed (see Fig. 6), whereas for green light ($\lambda = 513$ nm) the dependence of the quantum yield on Λ_F is shifted to higher reorganization energies (Fig. 7) compared to the case of the larger couplings $V_F = 25$ and 50 meV.

It should be noted that to cover a broader range of the spectrum of light with a fixed number of antenna chromophores, the resonance energies of the light-harvesting complexes should be very well separated. However, in this case the energy transfer between the antenna chromophores would be quite slow since this transfer is governed by the rates corresponding to the inverted regions of the Marcus parabola [32]. Then the dissipation comes into play and the energy of the absorbed photons is lost on its way from the antennas to the reaction center. The energy transfer rates and thus the efficiency of the system can be maximized in the case when the energy distance $\Delta E_i = E_{i+1} - E_i$ between the nearby light-harvesting complexes (labeled by indices $i + 1$ and i, with energies E_{i+1} and E_i) is equal to the corresponding reorganization energy Λ_F^i, that is, $\Delta E_i = E_{i+1} - E_i = \Lambda_F^i$. We note that for a system with identical antennas, the starlike configuration provides more energy to the reaction center than the linear one, although the latter one covers a narrower range of the sunlight spectrum.

VI. CONCLUSION

In this paper we have studied theoretical aspects of the operation of an artificial reaction center (a ferrocene-porphyrin-fullerene molecular triad) coupled to the complex of four light-harvesting molecules. We have analyzed two configurations of the antenna complex: (a) a star-shaped configuration, where each light-harvesting molecule is able to transfer energy directly to the centrally located reaction center, and (b) one in which the antenna molecules form a linear chain, which gradually transfers excitations from the high-energy antenna located in the far end to the antenna chromophore with the lowest energy. The last antenna chromophore in the chain is energetically connected to the reaction center. To be specific, we have considered the case in which the antenna complex is comprised of two molecules of bis(phenylethynyl)anthracene, absorbing blue photons ($\lambda = 450$ nm), and two molecules of borondipyrromethene, having an absorption maximum in the green region ($\lambda = 513$ nm). We have shown that the configuration with a linear arrangement of the antenna chromophores [configuration (b)] is able to convert blue and green photons to electricity with a quantum yield of order of $\sim$30% (over a wide range of wavelengths), whereas the energy of the red

photons, absorbed by the molecular triad itself ($\lambda = 620$ nm), is converted to a current with a quantum yield reaching the value of 90%. We have investigated dependences of the quantum yield on the Förster reorganization energy as well as on the Förster coupling constants between chromophores and have shown that the environment plays a significant role in facilitating the antenna-RC energy transfer, thus improving the light-harvesting function of the system. Overall, configuration (b) is more efficient than (a) in transferring energy to the reaction center. A similar conclusion takes place for the case of many antenna pigments coupled to the artificial reaction center.

We emphasize that the artificial photosystem analyzed in this work can be implemented with real light-harvesting components, such as porphyrin and BPEA-BDPY molecules. The excitonic (Förster) coupling strongly depends on the mutual distances and the orientations of the chromophores. Similar to the wheel-shaped antenna–reaction-center complex implemented in Ref. [6], the components of the photosystem can be placed at distances of the order 10 Å, which allows for a sufficiently strong Förster coupling between the antenna chromophores and the reaction center. At the same time, the chromophores comprising the light-harvesting complex retain their individual molecular features. The reorganization energy, another controlling parameter for energy transfer, is varied for the system under study. Namely, we numerically calculate both the light-induced electron current and the quantum yield as functions of the reorganization energy. This allows us to determine the value of the reorganization energy at which the system works with maximum optimal efficiency.

ACKNOWLEDGMENTS

We thank the RIKEN RICC for providing computing resources. P.K.G. was supported by JSPS Fellowship. F.N. acknowledges partial support from the Laboratory of Physical Sciences, National Security Agency, Army Research Office, National Science Foundation Grant No. 0726909, JSPS-RFBR Contract No. 09-02-92114, Grant-in-Aid for Scientific Research, MEXT Kakenhi on Quantum Cybernetics, and Funding Program for Innovative Research and Development on Science and Technology.

APPENDIX A: HAMILTONIAN

Here we describe the methods used in our work. We characterize the electrons in the states i (= D, P, P*, An1, An1*, An2, An2*, An3, An3*, An4, An4*, and A) by the Fermi operators $a_i^\dagger$ and a_i with the electron population operator $n_i = a_i^\dagger a_i$. Each electron state can be occupied by a single electron, as the spin degrees of freedom are neglected. Electrons in the leads (electrodes) are described by the Fermi operators $d_{k\alpha}^\dagger$ and $d_{k,\alpha}$, where $\alpha = L, R$ and k is an additional parameter that has the meaning of a wave vector in condensed matter physics. The number of electrons in the leads is determined by the operator $\sum_k N_{k\alpha}$, with $N_{k\alpha} = d_{k\alpha}^\dagger d_{k\alpha}$. The total Hamiltonian of the system is complicated. It includes the terms described below.

1. Eigenenergies and Coulomb interactions

This part of the Hamiltonian involved the eigenenergies of the electron states (i = D, P, P*, An1, An1*, An2, An2*, An3, An3*, An4, An4*, and A) and the Coulomb interactions between the electron states,

$$H_0 = \sum_i E_i n_i + u_P n_P n_{P^*} + u_{DP}(1-n_D)(1-n_P-n_{P^*}) - u_{DA}(1-n_D)n_A - u_{PA}(1-n_P-n_{P*})n_A. \tag{A1}$$

The symbols u_P, u_{DP}, u_{DA}, and u_{PA} represent the electrostatic interactions between the electron sites. We have assumed that the empty donor state D (with $n_D = 0$) and the empty photosensitive group $n_P + n_{P^*} = 0$ have positive charges. Therefore, $U_{DP} > 0$ because both D and P are positively charged and thus repulsive. The acceptor state A becomes negatively charged when it is occupied by an electron and thus $-U_{DA} < 0$ and $-U_{PA} < 0$. This attraction occurs when the acceptor A is occupied ($n_A = 1$) and the D and P states are both empty. Also, the acceptor state A is neutral when it is empty. The antenna pigments An1–An4 are coupled to each other and to the reaction center via dipole-dipole resonant coupling. They exchange only excitation energies but not electrons. Therefore, they always remain uncharged, so there are no Coulomb interactions between the antennas and other components of the photosystem.

2. Förster couplings

We consider the energy transfer between the reaction center P and the antenna complexes and also among the antenna complexes by introducing Förster coupling terms

$$H_{\text{Forster}} = -\sum_{kl} V_{kl} a_l^\dagger a_{l^*} a_{k^*}^\dagger a_k + \text{H.c.}, \tag{A2}$$

where the pair $\{k,l\}$ = {P, An1}, {P, An2}, {P, An3}, {P, An4}, {An1, An2}, {An2, An3}, and {An3, An4}. Here V_{kl} (1) determines the strength of the Förster coupling. We use the notation V_F instead of V_{kl} in the text.

3. Tunneling couplings to the leads

The electron tunneling from the left lead to the donor state and from the acceptor state to the right lead are both given by the Hamiltonian

$$H_{\text{tr}} = -\sum_k T_{kL} a_D^\dagger c_{kL} - \sum_k T_{kR} c_{kR}^\dagger a_A + \text{H.c.}, \tag{A3}$$

where $c_{k\alpha}^\dagger$ and $c_{k\alpha}$ are the electron creation and annihilation operators and α is the index for the leads. The Hamiltonian of the leads is given by

$$H_{LR} = \sum_\alpha \varepsilon_\alpha n_\alpha,$$

with

$$n_\alpha = \sum_k c_{k\alpha}^\dagger c_{k\alpha}.$$

4. Electron tunneling

Tunneling of electrons between components of the molecular triad is described by the Hamiltonian $H_{\rm tun}$,

$$H_{\rm tun} = -\sum_{l} \Delta_{l,l'} a_l^\dagger a_{l'} + \text{H.c.} \tag{A4}$$

Here $\Delta_{l,l'}$ is the strength of the tunneling coupling and the $\{l,l'\}$ indices refer to the pairs {D, P}, {D, P*}, {A, P}, and {A, P*}.

5. Light-induced excitations

This part of the Hamiltonian accounts for the interaction of light with the molecular triad and the antenna complexes. Under the rotating-wave approximation, the light-induced excitation processes can be described as

$$H_{\rm light} = -\sum_{k} F e^{i\omega_0 t} a_k^\dagger a_{k^*} + \text{H.c.}, \tag{A5}$$

where $k =$ P, An1, An2, An3, and An4 and the field amplitude

$$F = \mathcal{E}_{\rm ext} d_{kk^*},$$

where d_{kk^*} is the dipole moment of the k chromophore.

6. Coupling to a radiation heat bath and an Ohmic bath

Coupling the system to a radiation heat bath causes radiation leakage from the excited states. The following Hamiltonian accounts for this radiation leakage:

$$H_Q = -\sum_{\sigma} Q_{\sigma\sigma'} a_\sigma^\dagger a_{\sigma'} + \text{H.c.}, \tag{A6}$$

where $\{\sigma,\sigma'\}$ denotes the pairs of sites {D, P*}, {A, P}, {P, P*}, {An1,An1*}, {An2, An2*}, {An3, An3*}, and {An4, An4*}.

The operators for the radiation bath

$$Q_{\sigma\sigma'} = e\, x_{\sigma\sigma'} \times \mathcal{E}_{\rm rad} \tag{A7}$$

are proportional to the projection of the fluctuating electromagnetic field $\mathcal{E}_{\rm rad}$ along the direction of the corresponding dipole moment $d_{\sigma\sigma'} = e\ x_{\sigma\sigma'}$. The fluctuations of the blackbody radiation field are assumed to be isotropic.

The excited state of the photosensitive part of the molecular triad can be quenched by the electrode, namely, lose the excitation energy when interacting with the electrodes. We introduce $H_{\rm quench}$ to account for this energy-loss or quenching processes:

$$H_{\rm quench} = -Q_l a_l^\dagger a_{l'} + \text{H.c.}, \tag{A8}$$

where Q_l is the variable of the Ohmic bath and $\{l,l'\} =$ {P, P*}.

7. Interaction with the environment

We have taken into account the effects of a dissipative environment by the well-known system-reservoir model [19,32]:

$$H_{\rm env} = \sum_j \left[\frac{p_j^2}{2m_j} + \frac{m_j\omega_j^2}{2}\left(x_j + \frac{1}{2}\sum_i x_{ji} n_i\right)^2 \right], \tag{A9}$$

where x_j and p_j are the position and momentum, respectively, of the jth oscillator with effective masses m_j and frequencies ω_j and n_i are populations of electron sites in the system including the ground and excited states of antenna pigments. Here x_{ji} is a measure of the strength of the coupling between the electron subsystem and the environment. We characterize the phonon modes of the bath by the spectral functions $J_{ii'}(\omega)$, defined by

$$J_{ii'}(\omega) = \sum_j \frac{m_j\omega_j^3 (x_{ji} - x_{ji'})^2}{2} \delta(\omega - \omega_j). \tag{A10}$$

The spectral function $J_{ii'}$ is related to the reorganization energy $\Lambda_{ii'}$ for the $i \to i'$ transition by the following equation:

$$\Lambda_{ii'} = \int_0^\infty \frac{d\omega}{\omega} J_{ii'}(\omega) = \sum_j \frac{m_j\omega_j^2 (x_{ji} - x_{ji'})^2}{2}. \tag{A11}$$

APPENDIX B: MASTER EQUATIONS

The system under study can be characterized by the 256 eigenstates of H_0. We expressed all the operators described in preceding section in terms of the density operators $\rho_{\mu\nu} \equiv |\mu\rangle\langle\nu|$. To derive the time evolution of the diagonal elements $\rho_{\mu\mu} \equiv \rho_\mu$ of the density matrix $(\rho_{\mu\nu})$, we write the Heisenberg equation for the operators, with the subsequent averaging $\langle\rho_\mu\rangle$ over the environment fluctuations. Assuming (see, e.g., Refs. [19,20]) that the transition amplitudes (dipole-dipole elements V_F and electron tunneling rates Δ) of the photosystem are much less than the reorganization energies Λ and for the case of environment with sufficiently high temperature we obtain the master equations for the density matrix of the system [10,20],

$$\langle\dot\rho_\mu\rangle + \sum_\nu \gamma_{\nu\mu}\langle\rho_\mu\rangle = \sum_\nu \gamma_{\mu\nu}\langle\rho_\nu\rangle, \tag{B1}$$

where $\gamma_{\mu\nu}$ is the total relaxation matrix, which is the sum of six types of relaxation rates

$$\gamma_{\mu\nu} = \gamma_{\mu\nu}^{\rm tr} + k_{\mu\nu}^{\rm Forster} + k_{\mu\nu}^{\rm tun} + k_{\mu\nu}^{\rm light} + k_{\mu\nu}^{\rm rad} + k_{\mu\nu}^{\rm quench}. \tag{B2}$$

These relaxation rates will be described now.

1. Electron tunneling rates between the leads and the molecular triad

The first term of Eq. (B2), $\gamma_{\mu\nu}^{\rm tr}$, represents the relaxation rates due the couplings of the triad to the L and R electron reservoirs:

$$\begin{aligned}\gamma_{\mu\nu}^{\rm tr} = {}& \Gamma_L\{|a_{D;\mu\nu}|^2[1 - f_L(\omega_{\nu\mu})] + |a_{D;\nu\mu}|^2 f_L(\omega_{\mu\nu})\} \\ & + \Gamma_R\{|a_{A;\mu\nu}|^2[1 - f_R(\omega_{\nu\mu})] + |a_{A;\nu\mu}|^2 f_R(\omega_{\mu\nu})\},\end{aligned} \tag{B3}$$

where the resonant tunneling rates Γ_α ($\alpha =$ L,R) are related to the energy-independent tunneling factor by the equation

$$\Gamma_{L\alpha} = 2\pi \sum_k |T_{k\alpha}|^2 \delta(\omega - \epsilon_{k\alpha}), \tag{B4}$$

with $|T_{k\alpha}|$ the energy-independent tunneling factor. Here the electron reservoirs have been characterized by the Fermi distributions $f_\alpha(\omega)$,

$$f_\alpha(E_{k\alpha}) = \left[\exp\left(\frac{E_{k_B\alpha} - \mu_\alpha}{T}\right) + 1\right]^{-1}, \tag{B5}$$

with the temperature T ($k_B = 1, \hbar = 1$). The electrochemical potentials μ_L and μ_R are the controlling factors of the electron transition rates from the left lead to the donor state and from the acceptor state to the right lead.

2. Förster relaxation rates

Here $k_{\mu\nu}^{\text{Forster}}$ accounts for the excitation transfer rates from the antenna complexes to the reaction center and also among the antenna complexes. The excitation transition rates via the Förster mechanism can be derived with the methods described in Refs. [9,10,20],

$$\kappa_{\mu\nu}^{\text{Forster}} = \sum_{kl} \sqrt{\frac{\pi}{\Lambda_{kl}T}} |V_{kl}|^2 [|(a_l^\dagger a_{l^*} a_{k^*}^\dagger a_k)_{\mu\nu}|^2 + |(a_l^\dagger a_{l^*} a_{k^*}^\dagger a_k)_{\nu\mu}|^2] \exp\left[-\frac{(\omega_{\mu\nu} + \Lambda_{kl})^2}{4\Lambda_{kl}T}\right], \tag{B6}$$

where V_{kl} is the resonant Förster relaxation rate and Λ_{kl} stands for reorganization energy. We denote by $V_{kl} = V_F$ and $\Lambda_{kl} = \Lambda_F$ any combinations of k and l. The nonresonant exponential term of the above expression arises due to the different energy gaps of the reaction center and the accessory antenna complexes. Moreover, the nonresonant exponential terms depend on the reorganization energy.

3. Thermal tunneling rates

The matrix element $k_{\mu\nu}^{\text{tun}}$ of Eq. (B2) is responsible for the relaxation processes arising from thermal tunneling. These are given by

$$\kappa_{\mu\nu}^{\text{tun}} = \sum_{\sigma\sigma'} \sqrt{\frac{\pi}{\Lambda_{\sigma\sigma'}T}} |\Delta_{\sigma\sigma'}|^2 [|(a_\sigma^\dagger a_{\sigma'})_{\mu\nu}|^2 + |(a_\sigma^\dagger a_{\sigma'})_{\nu\mu}|^2] \exp\left[-\frac{(\omega_{\mu\nu} + \Lambda_{\sigma\sigma'})^2}{4\Lambda_{\sigma\sigma'}T}\right], \tag{B7}$$

where Δ is the resonant tunneling rate, $\omega_{\mu\nu}$ is the energy difference between the states μ and ν (acting as a thermodynamic gradient), and the reorganization energy Λ is the main guiding factor of the thermal tunneling rates $\kappa_{\mu\nu}^{\text{tun}}$. Details of the derivation can be found in Refs. [10,20].

4. Light-induced excitation rates

As in Ref. [10], the contribution $k_{\mu\nu}^{\text{light}}$ to the total relaxation matrix due to light-induced excitation processes is

$$\kappa_{\mu\nu}^{\text{light}} = \sum_k |F|^2 \sqrt{\frac{\pi}{\Lambda_{\sigma\sigma^*}T}} \left\{ |(a_\sigma^\dagger a_{\sigma^*})_{\mu\nu}|^2 \times \exp\left[-\frac{(\omega_{\mu\nu} + \omega_0 + \Lambda_{\sigma\sigma^*})^2}{4\Lambda_{\sigma\sigma^*}T}\right] + |(a_\sigma^\dagger a_{\sigma^*})_{\nu\mu}|^2 \exp\left[-\frac{(\omega_{\mu\nu} - \omega_0 + \Lambda_{\sigma\sigma^*})^2}{4\Lambda_{\sigma\sigma^*}T}\right] \right\}. \tag{B8}$$

This rate includes contributions from the transitions P $\to$ P*, An1 $\to$ An1*, An2 $\to$ An2*, An3 $\to$ An3*, and An4 $\to$ An4*.

5. Relaxation rates due to radiation leakage

Neglecting the effects of the environment on the radiation transitions, $k_{\mu\nu}^{\text{rad}}$ is given by

$$\kappa_{\mu\nu}^{\text{rad}} = \frac{2n}{3} \sum_{\sigma\sigma'} |d_{\sigma\sigma'}|^2 [|(a_\sigma^\dagger a_{\sigma'})_{\mu\nu}|^2 + |(a_\sigma^\dagger a_{\sigma'})_{\nu\mu}|^2] \times \left(\frac{\omega_{\mu\nu}}{c}\right)^3 \left[\coth\left(\frac{\omega_{\mu\nu}}{2T}\right) - 1\right], \tag{B9}$$

where n and $d_{\sigma\sigma'}$ stand for the refraction index and the dipole moment, respectively [10].

6. Lead-induced quenching rates of the excited states

The last term of Eq. (B2), $k_{\mu\nu}^{\text{quench}}$, describes the energy loss due to the quenching of the excited state of the photosensitive part of the triad:

$$\kappa_{\mu\nu}^{\text{quench}} = \alpha_p [|(a_P^\dagger a_{P^*})_{\mu\nu}|^2 + |(a_P^\dagger a_{P^*})_{\nu\mu}|^2] \times \omega_{\mu\nu} \left[\coth\left(\frac{\omega_{\mu\nu}}{2T}\right) - 1\right]. \tag{B10}$$

APPENDIX C: CURRENT AND EFFICIENCY

1. Electron current

For weak couplings, the electron flowing (particle current) between the leads and the molecular triad is given by

$$I_e = I_R = \left(\frac{d}{dt}\right) \sum_k \langle c_{kR}^\dagger c_{kR} \rangle.$$

We derive the equation of the current in terms of the density-matrix elements,

$$I_e = \Gamma_R \sum_{\mu\nu} |a_{A;\mu\nu}|^2 [1 - f_R(\omega_{\nu\mu})] \langle \rho_\nu \rangle - \Gamma_R \sum_{\mu\nu} |a_{A;\mu\nu}|^2 f_R(\omega_{\nu\mu}) \langle \rho_\mu \rangle. \tag{C1}$$

2. Absorbed energy

The total amount of energy absorbed per unit time $\mathcal{E}_{\text{photon}}$ by the molecular triad and antenna chromophores is

$$\mathcal{E}_{\text{photon}} = \sum_\sigma \omega_0 |F|^2 \sqrt{\frac{\pi}{\Lambda_{\sigma\sigma^*}T}} \sum_{\mu\nu} |(a_\sigma^\dagger a_\sigma)_{\mu\nu}|^2 \langle \rho_\mu - \rho_\nu \rangle \times \left(\exp\left[-\frac{(\omega_{\mu\nu} - \Lambda_{\sigma\sigma^*} + \omega_0)^2}{4\Lambda_{\sigma\sigma^*}T}\right] - \exp\left[-\frac{(\omega_{\mu\nu} - \Lambda_{\sigma\sigma^*} - \omega_0)^2}{4\Lambda_{\sigma\sigma^*}T}\right] \right), \tag{C2}$$

where σ = P, An1, An2, An3, and An4.

3. Power-conversion efficiency

The power-conversion efficiency of the system is the ratio of the output E_{output} and the input E_{input} energies,

$$\eta = \frac{E_{\text{output}}}{E_{\text{input}}} = \frac{\mathcal{E}_{\text{pump}}}{\mathcal{E}_{\text{photon}}} = \frac{I_R(\mu_R - \mu_L)}{\mathcal{E}_{\text{photon}}}. \tag{C3}$$

The quantum yield is defined as

$$\Phi = \frac{n_{\text{pump}}}{N_{\text{photon}}} = \eta \frac{\hbar\omega_0}{\mu_R - \mu_L}. \tag{C4}$$

[1] R. E. Blankenship, *Molecular Mechanisms of Photosynthesis* (Blackwell Science, Oxford, 2002).

[2] H. V. Amerongen, L. Valkunas, and R. Van Grondelle, *Photosynthetic Excitons* (World Scientific, Singapore, 2000).

[3] D. Kuciauskas, P. A. Liddell, S. Lin, T. E. Johnson, S. J. Weghorn, J. S. Lindsey, A. L. Moore, T. A. Moore, and D. Gust, J. Am. Chem. Soc. **121**, 8604 (1999).

[4] H. Imahori, J. Phys. Chem. B **108**, 6130 (2004).

[5] H. Imahori, Bull. Chem. Soc. Jpn. **80**, 621 (2007).

[6] G. Kodis, Y. Terazono, P. A. Liddell, J. Andréasson, V. Garg, M. Hambourger, T. A. Moore, A. L. Moore, and D. Gust, J. Am. Chem. Soc. **128**, 1818 (2006).

[7] D. Gust, T. A. Moore, and A. L. Moore, Acc. Chem. Res. **42**, 1890 (2009).

[8] A. M. Ferreira and D. Bashford, J. Am. Chem. Soc. **128**, 16778 (2006).

[9] P. K. Ghosh, A. Yu. Smirnov, and F. Nori, J. Chem. Phys. **131**, 035102 (2009).

[10] A. Yu. Smirnov, L. G. Mourokh, P. K. Ghosh, and F. Nori, J. Phys. Chem. C **113**, 21218 (2009); P. K. Ghosh, A. Yu. Smirnov, and F. Nori, J. Chem. Phys. **134**, 244103 (2011).

[11] M. Mohseni, P. Rebentrost, S. Lloyd, and A. Aspuru-Guzik, J. Chem. Phys. **129**, 174106 (2008).

[12] M. B. Plenio and S. F. Huelga, New J. Phys. **10**, 113019 (2008).

[13] P. Rebentrost, M. Mohseni, I. Kassal, S. Lloyd, and A. Aspuru-Guzik, New J. Phys. **11**, 033003 (2009).

[14] F. Caruso, A. W. Chin, A. Datta, S. F. Huelga, and M. B. Plenio, J. Chem. Phys. **131**, 105106 (2009).

[15] Y. Terazono, G. Kodis, P. A. Liddell, V. Garg, T. A. Moore, A. L. Moore, and D. Gust, J. Phys. Chem. B **113**, 7147 (2009).

[16] Y. Terazono, G. Kodis, K. Bhushan, J. Zaks, C. Madden, A. L. Moore, T. A. Moore, G. R. Fleming, and D. Gust, J. Am. Chem. Soc. **133**, 2916 (2011).

[17] D. Gust, T. A. Moore, and A. L. Moore, Acc. Chem. Res. **42**, 1890 (2009).

[18] R. W. Wagner and J. S. Lindsey, J. Am. Chem. Soc. **116**, 9759 (1994).

[19] D. A. Cherepanov, L. I. Krishtalik, and A. Y. Mulkidjanian, Biophys. J. **80**, 1033 (2001).

[20] A. Yu. Smirnov, L. G. Mourokh, and F. Nori, J. Chem. Phys. **130**, 235105 (2009).

[21] P. Rebentrost, M. Stopa, and A. Aspuru-Guzik, Nano Lett. **10**, 2849 (2010).

[22] A. Yu. Smirnov, L. G. Mourokh, and F. Nori, Phys. Rev. E **77**, 011919 (2008).

[23] E. Collini and G. D. Scholes, Science **323**, 369 (2009).

[24] G. Panitchayangkoon, D. Hayes, K. A. Fransted, J. R. Caram, E. Harel, J. Wen, R. E. Blankenship, and G. S. Engel, Proc. Natl. Acad. Sci. USA **107**, 12766 (2010).

[25] Y.-C. Cheng and G. R. Fleming, Annu. Rev. Phys. Chem. **60**, 241 (2009).

[26] M. Yang and G. R. Fleming, Chem. Phys. **282**, 163 (2002).

[27] H. Imahori, H. Yamada, Y. Nishimura, I. Yamazaki, and Y. Sakata, J. Phys. Chem. B **104**, 2099 (2000).

[28] K. Weber, L. Hockett, and S. Creager, J. Phys. Chem. B **101**, 8286 (1997).

[29] H. Imahori, H. Yamada, D. M. Guldi, Y. Endo, A. Shimomura, S. Kundu, K. Yamada, T. Okada, Y. Sakata, and S. A. Fukuzumi, Angew. Chem. Int. Ed. **41**, 2344 (2002).

[30] H. Imahori, N. V. Tkachenko, V. Vehmanen, K. Tamaki, H. Lemmetyinen, Y. Sakata, and S. Fukuzumi, J. Phys. Chem. A **105**, 1750 (2001).

[31] V. Urboniene, O. Vrublevskaja, G. Trinkunas, A. Gall, B. Robert, and L. Valkunas, Biophys. J. **93**, 2188 (2007).

[32] R. A. Marcus and N. Sutin, Biochim. Biophys. Acta **811**, 265 (1985).